Nanoscale

Accepted Manuscript

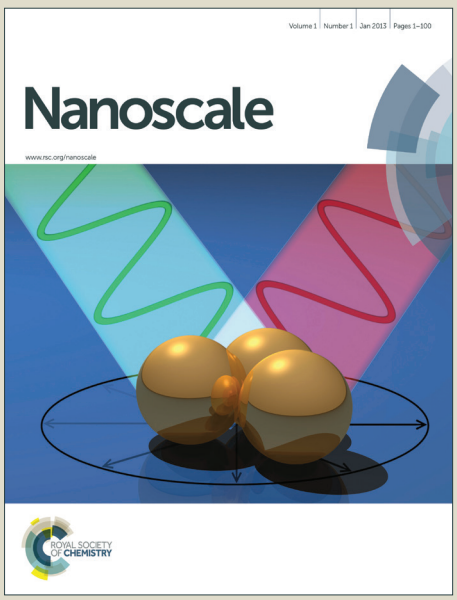

ROYAL SOCIETY OF CHEMISTRY

www.rsc.org/nanoscale

A Mo Nanoscrew Formed by Crystalline Mo Grains with High Conductivity and Excellent Field Emission Properties

Yan Shen, Ningsheng Xu, Shaozhi Deng*, Yu Zhang, Fei Liu, and Jun Chen

Abstract

A novel screw-like molybdenum nanostructure has been synthesized based on a simple thermal vapor deposition method. Each thread circle of a nanoscrew is formed by several crystalline Mo grains, which have a certain deflection with each other. The growth mechanism is described as a spiral growth mode, which depends heavily on the degree of supersaturation (σ) of deposited Mo vapors. The electrical property measurements and field emission properties on single Mo nanoscrew show that its electrical conductivity should reach 3.44×10^{4} –7.74×10^{4} Ω^{-1} cm^{-1} and its maximum current get 15.8 μA. Mo nanoscrews film is also proved to have very excellent field emission properties in different voltage driver modes. The largest emission current densities can get 106.39 mA cm^{-2} in DC voltage driver mode and 0.66 A cm^{-2} in pulsed mode. Low turn-on field, good sites distribution and remarkable emission stability also can be recorded. These experimental results show that the high conductive molybdenum nanoscrews should be a potential application as cold cathode material for the high current vacuum electron devices, while it is a kind of low cost and controllable repetitive preparation method compared to the perfect single crystalline Mo nanostructure.

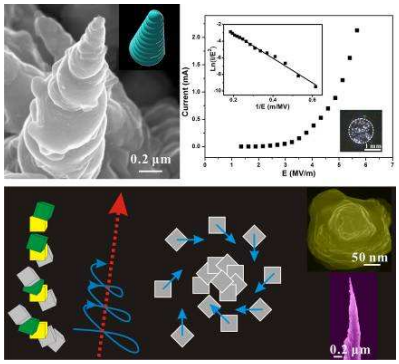

Cite this: DOI: 10.1039/c0xx00000x

www.rsc.org/xxxxxx

ARTICLE TYPE

A Mo Nanoscrew Formed by Crystalline Mo Grains with High Conductivity and Excellent Field Emission Properties

Yan Shen [a], Ningsheng Xu [a], Shaozhi Deng*[a], Yu Zhang [a], Fei Liu [a], and Jun Chen [a]

Received (in XXX, XXX) Xth XXXXXXXXX 20XX, Accepted Xth XXXXXXXXX 20XX

DOI: 10.1039/b000000x

A novel screw-like molybdenum nanostructure has been synthesized based on a simple thermal vapor deposition method. Each thread circle of a nanoscrew is formed by several crystalline Mo grains, which have a certain deflection with each other. The growth mechanism is described as a spiral growth mode, which depends heavily on the degree of supersaturation (σ) of deposited Mo vapors. The electrical property measurements and field emission properties on single Mo nanoscrew show that its electrical conductivity should reach 3.44×10^4 –7.74×10^4 Ω^{-1} cm^{-1} and its maximum current get 15.8 μA. Mo nanoscrews film is also proved to have very excellent field emission properties in different voltage driver modes. The largest emission current densities can get 106.39 mA cm^{-2} in DC voltage driver mode and 0.66 A cm^{-2} in pulsed mode. Low turn-on field, good sites distribution and remarkable emission stability also can be recorded. These experimental results show that the high conductive molybdenum nanoscrews should be a potential application as cold cathode material for the high current vacuum electron devices.

1. Introduction

Nanotechnology development unceasingly shows humans new structures with novel functions and properties, which lay the foundation for newborn device applications. Since carbon nanotubes were reported in 1991,[1] various nanostructures have been paid considerable attention due to their geometrical characteristics and the applications. Nanowires [2–7] with being to construct characteristic, have been studied in field effect transistor (FET),[8] electronic and optoelectronic devices,[9] logic gates,[10] nanolasers,[11] and piezoelectric nanogenerators.[12] Nanobelts, with large surface area and perfect crystallinity, could be doped with different elements and used for fabricating nanosensors.[13] Nanocables, with one-dimensional features of both nanowire and nanotube in the axial direction, have been promised great potential for electronic transportation.[14] Graphene and its analogues, with monolayer atom thick, have been proved to own excellent electrical transport and mechanical characteristics, for used in metallic transistor, sensors, transparent electrodes and so on.[15,16] In addition to these, nanowalls with vertical orientation and large surface area,[17] nanotips with sharp tip and thick bottom,[18] nanostars with solid core and protruding prolate tips,[19] and nanosprings with helical structure and periodic arrangement,[20] have also been demonstrated interesting physical properties and potential applications. New-style structures await to be added to the growing nanomaterials family. Here, we report a screw-like nanostructure formed by crystalline molybdenum grains, which shows very high conductivity and excellent field emission properties.

Molybdenum has characteristics of high melting point, high conductivity and high temperature stability,[21,22] and has been applied to the field electron emission material, which is conducive to obtain the stability of the electron emission and high emission current density. Since 1976, the Mo micro-cone has been used as field emitter arrays for the cold cathode.[23] In the last ten years, people focus on molybdenum and its oxides nanostructure.[7, 24–27] However, the design and synthesis of the molybdenum nanostructure with excellent performance of conductivity and emission current density is still a challenging issue. In this work, the Mo nanoscrews are synthesized using a thermal vapor deposition technique based on our previous study.[25,27] The conductivity and field emission properties in both direct-current (DC) and pulsed voltage driver mode have been investigated. We found that this kind of Mo nanoscrew shows the excellent conductivity and field emission properties for potential application in the cold cathode.

2. Experimental

The basic reactions have been described in our previous paper,[25,27] which we used in the present study to get pure molybdenum. The Mo source reacted with residual oxygen in the system to give rise to MoO_2 vapor over 1350 ℃. Then, the Mo atoms coming from the decomposition of MoO_2 deposited on the substrate over 1155 ℃. Molybdenum nanoscrews were grown on stainless steel substrates by heating a Mo boat to 1350 ℃ under constant flow of argon and interrupted flow of hydrogen for more than 15 min in a vacuum chamber.

Circular stainless steel substrates (Φ 1.6 mm × 0.3 mm) and

Mo boat (117 mm × 15 mm × 0.3 mm) were washed with acetone and then with alcohol for more than 15 min in an ultrasonic bath respectively. Then, the boat and substrates were placed in the center of vacuum chamber (Φ 300 mm × 450 mm) with keeping them about 3 mm away from each other. When the vacuum reached below approximately 5×10^{-2} torr evacuated using a mechanical pump, a constant flow of high purity argon gas (99.99%; 80 sccm, standard cubic centimeters per minute) and a flow of high purity hydrogen gas (99.99%; 80 sccm) were introduced into the system. The temperature of Mo boat was then increased over 1350 ℃ gradually at a rate of 50 ℃ min^{-1} and kept at that temperature for more than 15 min. During the holding time, the hydrogen gas was interrupted to guarantee enough MoO_2 vapor could be produced and the subsequent decomposition reaction could happen. Finally, the temperature was allowed to decrease slowly to room temperature and the synthesis of Mo nanoscrews was completed.

The nanoscrews were analyzed by SEM (Zeiss Supra55 operated at 10 kV), XRD (Rigaku RINT2400), TEM (JEM-2010 operated at 200 kV), and EDX (installed in Zeiss Supra55).

The electrical transport and field emission measurements of the individual nanoscrews were carried out using a micro-point anode in situ in a modified SEM system (Zeiss Supra55 operated at 10 kV and 4×10^{-6} torr), the details of which were described in our previous reports.[27] The field emission performance of the nanoscrews film was studied in an ultra high vacuum system (7.5×10^{-9} torr) at room temperature. The samples as the cathodes were all about 0.02 cm^2 and in disc form. Under direct-current (DC) voltage driver mode, thick ITO glass (Φ 20 mm × 3 mm) as the anode was kept about 200 μm away from the cathode. A charge coupled device (CCD) camera was used to record the distribution of the field emission sites. In pulsed voltage driver mode, a pulse power (CDGD-MCCD2 operated at 2000 Hz) was employed for the input anode voltage. An external sampled resistance of 20 Ω was used. An oscilloscope (Tektronix TDS-210) was supplied to record the input and output waveforms.

3. Results and Discussion

3.1 Characteristics of Mo nanoscrew

Figure 1a shows the top-view SEM image of molybdenum nanoscrews. The nanoscrews are seen to be distributed all over the substrate surface. The average density is estimated to be 5×10^7 cm^{-2}. Figure 1b gives the side-view SEM image of the sample. The length of the nanoscrew ranges from 2 to 6 μm. The nanoscrews have a maximum diameter over 500 nm on the bottom and a minimum diameter over 50 nm at the tip. From the high-magnification SEM images of the area C and D in Figure 1b, one can see different individual nanoscrew. A representative individual in Figure 1e shows that the Mo nanoscrew is formed by screwy grains along its longitudinal growth direction. The morphology of adjacent screw thread is cyclically similar to each other. In addition, the average number of thread circles of each nanoscrew is about 10. A typical XRD pattern of the nanoscrews is shown in Figure 1f. All the peaks can be indexed to metallic Mo of a pure bcc structure with a cell constant of $a = b = c = 3.14$ Å (JCPDS: 42-1120), indicating that the product we prepared is pure molybdenum.

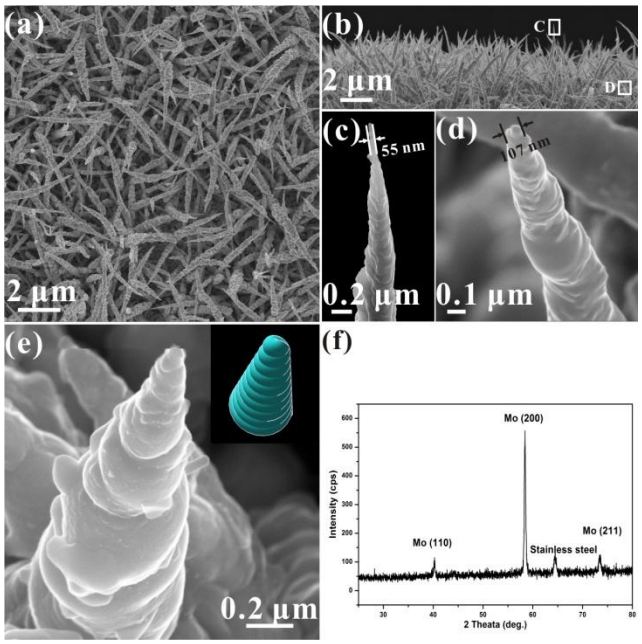

Figure 1. a) Top-view SEM image of molybdenum nanoscrews. b) Side-view SEM image of Mo nanoscrews. c, d) High-magnification SEM images of the area C and D in (b) respectively. e) High-magnification SEM image of individual nanoscrew, and the inset is the corresponding geometrical model. f) XRD spectrum of Mo nanoscrews.

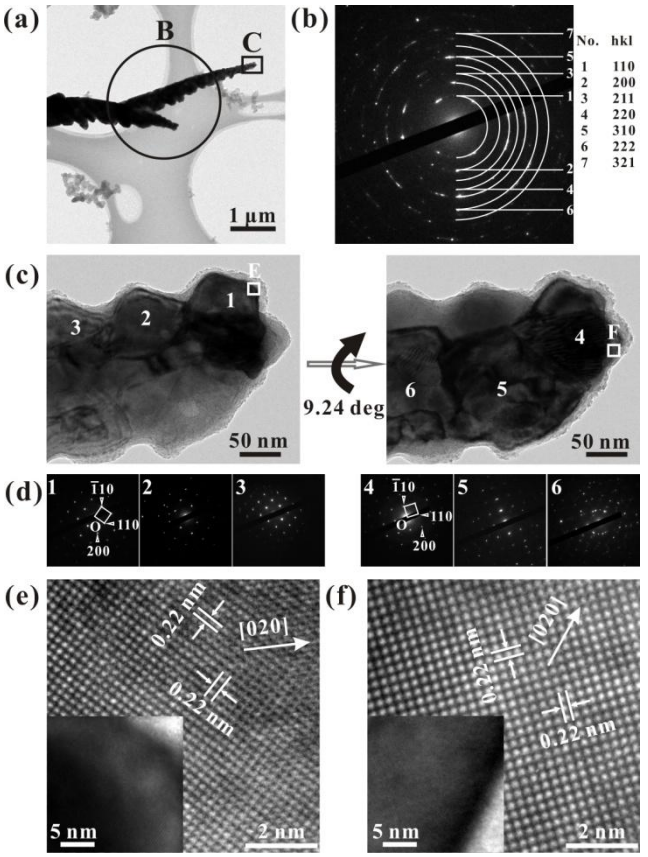

Figure 2. a) Typical TEM image of molybdenum nanoscrews. b) Selected-area electron diffraction (SAED) patterns of the area B in (a). c) TEM images of the area C in (a) with little rotation. d)

The corresponding SAED patterns of different areas 1-6 marked in (c). e,f) HRTEM images of the areas E and F in (c) respectively.

TEM technique has been employed to study the detailed structure of the Mo nanoscrew. First, low-magnification TEM image is emerged in Figure 2a, which clearly reveals that the nanoscrew has a sharp tip and thick bottom, with a screwy growth happened on the body. Selected-area electron diffraction (SAED) of the area B patterns the Debye-Scherrer concentric rings of (110), (200), (211), and so on (Figure 2b), confirming that the Mo nanoscrew was in a polycrystalline structure. Figure 2c shows high-magnification TEM images of the top area C of the nanoscrew in Figure 2a, taken with different rotations. It shows that each thread circle of the nanoscrew is composed of several crystalline Mo grains. The grains in the same circle have a certain deflection with each other. However, the grains in different circles with longitudinal direction adjacent present roughly the same size and morphology, such as the marked areas 1, 2 and 3. The corresponding SAED patterns were also analyzed, and indicate that the marked grains 1, 2 and 3 have perfect single crystalline structure and consistent deflecting direction (Figure 2d). High-resolution TEM (HRTEM) image (Figure 2e) of the area E in Figure 2c further verifies that the marked gain is crystalline, with the mean lattice spacing being 0.22 nm between two adjacent crystalline planes, which is consistent with the {110} planes of the body-centered cubic (bcc) molybdenum. The nucleation direction can be determined as along [020]. Moreover, by rotating the nanoscrew to a proper orientation, the SAED patterns of Mo grains in areas 4 and 5 (Figure 2d) could be sharp and ordered. The corresponding HRTEM image (Figure 2f) also reveals that the grains in these areas are bcc Mo with nucleation direction along [020]. Mo grains in areas 4 and 5 were examined to have the same deflection, but a certain angle compared to the grains 1, 2 and 3 (Figure 2c), which indicated the existence of a polycrystalline structure in the nanoscrews. The growth direction of the Mo nanoscrew could be obtained by indexing all the nucleation directions of the crystalline Mo grains appeared in one screwy thread circle.

3.2 Growth mechanism

Based on the structure characterization above, we shall discuss the growth mechanism of the Mo nanoscrews. From Figure 3a, one can see that most Mo grains have a normal particle size of approximately 50 nm. The nucleation of each grain didn't have enough growing energy and had to stop at this scale. From the top-view SEM image of an individual nanoscrew (Figure 3b), screwy thread can be observed, and it means that a spiral growth existed during the process. Figure 3c gives the corresponding schematic diagrams. The growth direction of the Mo nanoscrew (indicated by the dotted arrow) can be presented as the vector sum of all the different nucleation directions (indicated by the solid arrows). In this case, we should understand by a modified vapor-solid (VS) mechanism based on the oxidation of molybdenum and the subsequent decomposition reaction,[25,27] which the growth of the nanoscrews comes from the screw-type dislocations in the bottom particles,[28] and closely relates to the degree of supersaturation (σ) of the deposited Mo vapor.[29]

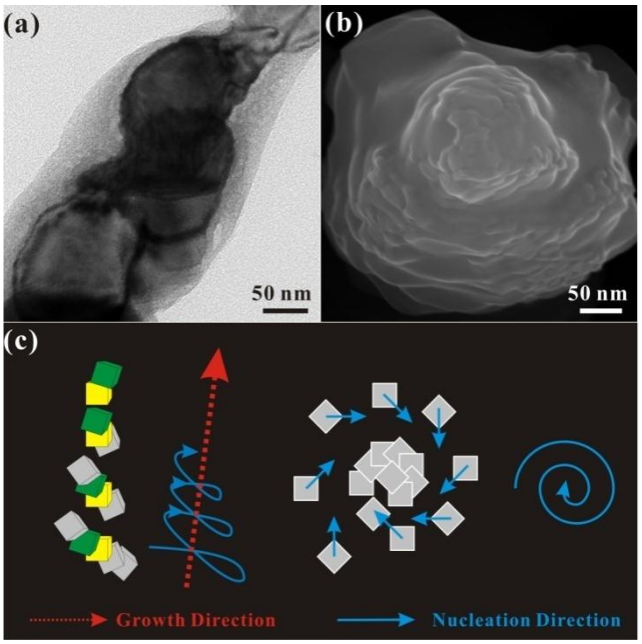

Figure 3. a) TEM image of the tip of individual nanoscrew. b) Top-view SEM image of another individual nanoscrew. c) Schematic diagrams of Mo nanoscrew formed by crystalline Mo grains.

Burton, Cabrera and Frank (BCF) theory predicted that the dependence of the spiral growth rate R_{sp} can be:[28]

$$R_{sp} = av\exp(-\frac{E_a}{kT})\frac{\sigma^2}{\sigma_1}\tanh\frac{\sigma_1}{\sigma} \quad (1)$$

where R_{sp} is the spiral growth rate, a is the step height of the Mo (020) plane, v is the frequency factor, E_a is the evaporation energy per atom, and σ_1 is the critical supersaturation. For low supersaturations ($\sigma \ll \sigma_1$), (tanh σ_1/σ) in Equation (1) is nearly equal to unity. Thus, R_{sp} can be approximated to parabolic form as follows:

$$R_{sp} = av\exp(-\frac{E_a}{kT})\frac{\sigma^2}{\sigma_1} \quad (2)$$

While in another growth mode, which called layered nucleus mode, the growth rate in the multinucleation $R_{m\text{-}nuc}$ can be:[30,31]

$$R_{m-nuc} = aI_0^{1/3}\exp\left[-\frac{\pi(\frac{\gamma'}{kT})^2}{3\sigma}\right]v^{2/3} \quad (3)$$

where I_0 and γ' are the pre-exponential factor and step energy per atom, respectively. v is step velocity, and $v=v_\infty tanh(\sigma_1/\sigma)$,where v_∞ is the step velocity of a single step on an infinite area. For low supersaturation ($\sigma \ll \sigma_1$), tanh (σ_1/σ) is nearly equal to unity, v can be approximated to be v_∞. So the multinucleation growth rate $R_{m\text{-}nuc}$ defined by Equation (3) can be expressed as:

$$R_{m-nuc} = aI_0^{1/3}\exp\left[-\frac{\pi(\frac{\gamma'}{kT})^2}{3\sigma}\right]v_\infty^{2/3} \quad (4)$$

It can be found that the σ of Mo vapor have much effect on both spiral growth rate and layered nucleus growth rate. If the value of σ is quite low ($\sigma \ll \sigma_1$), the spiral growth rate R_{sp} increases proportionally to σ^2, which is much larger than the latter one in this range, and it indicates that the growth of Mo

nanoscrews tends to a spiral mode. On the contrary, if σ becomes enough high, the layered nucleus mode will dominate the whole growing process. Besides that, with considering the inadequate growth time and not high enough temperature, it is very difficult for the newly decomposed Mo to select the most suitable location and grow with low energy. This may explain the scale limit of Mo grains and the existing of defects (such as stacking faults and dislocations), which make the Mo nanoscrew present complicated polycrystalline structure.

3.3 Conductivity

It is very interesting to have clear insight into the electrical properties of the Mo nanoscrews. We selected five individual nanoscrew samples with different length and diameters to proceed our measurements. The corresponding *I-V* curves are almost linear. It means that there were good Ohmic contacts existing between the Mo nanoscrews and the substrate, and between the W microprobe and the contacting surfaces. The individuals with shorter length and larger diameter typically have smaller resistance (see Figure 4 and Table 1).

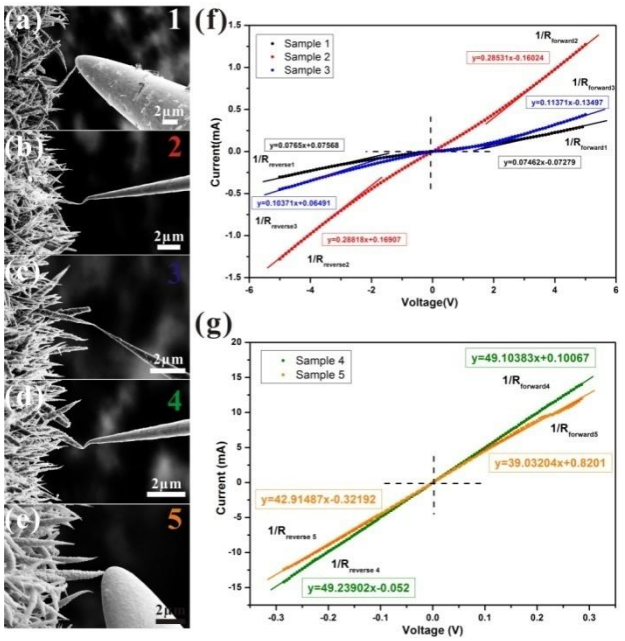

Figure 4. a–e) SEM images showing the W microprobe in contact with the tip of five different Mo nanoscrew samples for electrical transport measurements. f,g) The corresponding *I-V* characteristic curves for Sample 1–3 and for Sample 4,5, respectively. The resistance for forward applied voltage ($R_{forward}$) and the resistance for reverse applied voltage ($R_{reverse}$) were calculated by fitting the *I-V* plots (listed in Table 1).

Table 1. The electrical transport properties of different individual molybdenum nanoscrew samples

Mo Nanoscrew	1	2	3	4	5
$1/R_{forward}$ [kΩ^{-1}]	0.0746	0.2853	0.1137	49.1038	39.0320
$R_{forward}$ [kΩ]	13.4	3.5	8.8	0.0204	0.0256
$1/R_{reverse}$ [kΩ^{-1}]	0.0765	0.2882	0.1037	49.2390	42.9149
$R_{reverse}$ [kΩ]	13.1	3.5	9.6	0.0203	0.0233
$R_{average}$ [Ω]	13300	3500	9200	20.337	24.461

For further calculating the electrical conductivity of single Mo nanoscrews, the intrinsic resistance of substrate and circuit loop, and the contact resistance between nanoscrew and substrate should be eliminated. A thinner nanoscrew with length (L) of ~4 μm, tip diameter (d_1) of ~ 62 nm, root diameter (d_2) of ~0.476 μm, and a thicker nanoscrew with L~2 μm, d_1 ~0.131 μm, d_2 ~0.612 μm, were chosen to have the electrical conductivity analysis, respectively. As shown in Figure 5a and 5b, first, the W microprobe contacted the tip area A of the nanoscrews. Second, the W microprobe touched the bottom area B of the individuals. By fitting the corresponding *I-V* plots, the average inherent body resistance R of the chosen samples can be obtained as 69.09 Ω and 5.217 Ω respectively (see Table 2). The corrseponding equivalent circuit diagram is given in Figure 5c. Here, only the contact resistance between the W microprobe and the nanoscrew is impossible to be completely eliminated, since the contact in each measurement is different. Considering the resistance for forward applied voltage is nearly equal to the resistance for the reverse one, we may ignore such difference.

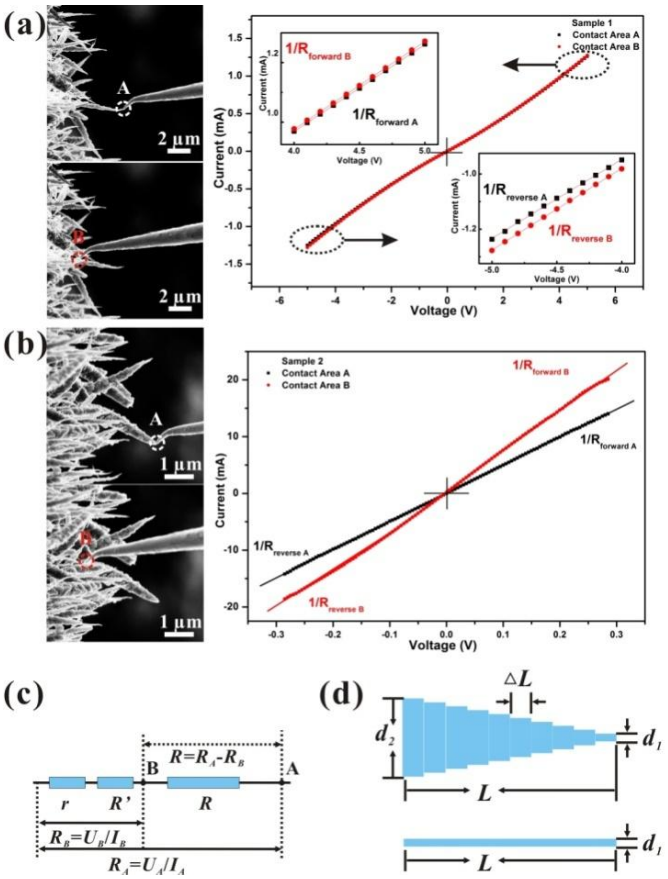

Figure 5. a) SEM images showing the W microprobe in contact with area A and B of a thinner Mo nanoscrew sample and the corresponding current versus voltage (*I–V*) characteristic curves, during the electrical conductivity measurement. b) SEM images and *I–V* curves of a thicker Mo nanoscrew sample. c) Schematic circuit diagram for calculating the body resistance R of Mo nanoscrew, where R' is the root resistance of the sample, and r is the intrinsic resistance of substrate and circuit loop. d) Schematic diagram for the calculation of the electrical conductivity of individual Mo nanoscrews.

Table 2. The calculation of intrinsic resistance of different individual molybdenum nanoscrew samples

Thinner Sample	$1/R_{forward}$ [$k\Omega^{-1}$]	$R_{forward}$ [kΩ]	$1/R_{reverse}$ [$k\Omega^{-1}$]	$R_{reverse}$ [kΩ]	$R_{average}$ [Ω]
Top	0.2924	3.4200	0.2863	3.4935	3456.7
Bottom	0.2944	3.3972	0.2960	3.3780	3387.6
Nanoscrew					69.09
Thicker Sample	$1/R_{forward}$ [$k\Omega^{-1}$]	$R_{forward}$ [kΩ]	$1/R_{reverse}$ [$k\Omega^{-1}$]	$R_{reverse}$ [kΩ]	$R_{average}$ [Ω]
Top	49.1038	0.02037	49.2390	0.02031	20.337
Bottom	69.7429	0.01434	62.8854	0.01590	15.120
Nanoscrew					5.217

Figure 5d introduces a geometric model to calculate the electrical conductivity of individual Mo nanoscrews. The body resistance R of nanoscrew was considered as the sum of the values of each screwy thread circle. Assuming that diameters of these circles are equidifferent distributed and the screw pitch is constant, the screw pitch ΔL and the difference between adjacent diameters Δd are described as:

$$\Delta L = \frac{L}{N}, \qquad \Delta d = \frac{d_2 - d_1}{N-1} \tag{5}$$

where L is the length of Mo nanoscrew, N is the number of circles, d_1 is the tip diameter, and d_2 is the root diameter. The body resistance R of Mo nanoscrew can be taken as a sum of the parallel circles, and should be expressed as:

$$\begin{aligned} R &= R_{d_2} + R_{d_2-\Delta d} + \cdots + R_{d_2-(N-2)\Delta d} + R_{d_1} \\ &= \frac{4\Delta L}{\kappa\pi d_2^2} + \frac{4\Delta L}{\kappa\pi (d_2-\Delta d)^2} + \cdots + \frac{4\Delta L}{\kappa\pi [d_2-(N-2)\Delta d]^2} + \frac{4\Delta L}{\kappa\pi d_1^2} \\ &= \frac{L}{\kappa S} \end{aligned} \tag{6}$$

So the electrical conductivity (κ) of individual Mo nanoscrew can be finally given:

$$\kappa = \frac{4L}{\pi RN}\left\{\frac{1}{d_2^2} + \left[\frac{(N-1)}{(N-2)d_2 + d_1}\right]^2 + \cdots + \left[\frac{(N-1)}{d_2 + (N-2)d_1}\right]^2 + \frac{1}{d_1^2}\right\} \tag{7}$$

By substituting the parameters of the chosen samples into Equation (7), the values κ of different individuals are estimated as 3.44×10^4 Ω^{-1} cm^{-1} and 7.74×10^4 Ω^{-1} cm^{-1} respectively. The electrical conductivity for single Mo nanoscrew is an order of magnitude less than the molybdenum bulk material (approximately 1.946×10^5 Ω^{-1} cm^{-1}),[22] and larger than most metallic or semi-conductive nanostructures reported (listed in Table 3).

The screwy structure may contribute to its excellent electrical transport property. To verify that, we supposed a Mo nanorod having uniform diameter d_1 and the same length L with Mo nanoscrew, as given by Figure 5d. The theoretic body resistance R^* of the assumed nanorod can be described as follows:

$$R^* = \frac{L}{\kappa S} = \frac{4L}{\kappa\pi d_1^2} \tag{8}$$

Using the electrical conductivities of the obtained by the calculation model, the resistances of the two shape-changed samples may be estimated as 385.15 Ω and 19.17 Ω respectively, which are much larger than the experimental values. This supplies an evidence that Mo nanoscrews have a better electric transport property than other one-dimentional nanostructures. It is worth noting that the defects in nanoscrews could resist the movement of electrons and reduce the conductivity, but such polycrystalline structure has gotten a high electrical transport property.

Table 3. The electrical conductivities for various individual nanostructure materials

Material	Nanostructure	Intrinsic Conductivity κ [Ω^{-1} cm^{-1}]
C	Tube [32]	$0.172\sim19.6\times10^4$
Cu_2S	Wire [33]	0.1
CuO	Wire [34]	7.8
CdS	Wire [35]	0.82
ZnO	Agave-like [36]	3.37×10^3
	Hierarchical [36]	2.57
	Pencil-like [36]	0.0144
$W_{18}O_{49}$	Wire [37]	2.58
WO_2	Wire [38]	20.6
WO_3	Wire [38]	9.7
B	Wire [39]	0.03
	Tube [40]	36.85
	Sword [41]	0.0158
B_4C	Wire [42]	0.051
Ge	Taper [43]	3.33
	Wire [43]	0.012
Mo	Screw-thinner	3.44×10^4
	Screw-thicker	7.74×10^4

3.4 Field emission

We have measured the field emission properties of individual Mo nanoscrews. Figure 6a shows the current versus electric field (I–E) characteristic curves and the corresponding F-N plots at high electric field region (inset) of four single Mo nanoscrews. The vacuum gap was kept about ~2 μm. Table 4 lists the geometrical parameters of the individuals and their field emission properties recorded, one can see that those nanoscrews with higher aspect ratio ($2L/d_1$) always have lower turn on field (E_{to}). In addition, the samples with larger root diameter d_2 present higher emission current typically. The maximum field emission current was recorded as 15.8 μA, which is much larger than the value of individual CNT (approximately 1 μA).[44]

Table 4. Geometric characteristics and field emission properties of different individual molybdenum nanoscrew samples

Sample	Length [μm]	d_1 [μm]	d_2 [μm]	L/r_1	I_{max} [μA]	J_{max} [$\times10^4$A cm^{-2}]
1	4	0.125	0.476	64	1.18	0.96
2	4. 5	0.085	0.568	106	4.96	8.74
3	3.8	0.072	0.729	106	6.5	15.96
4	5.8	0.100	1.311	116	15.8	20.12

As is known, the apex of the structure with greater length and smaller tip diameter could produce higher local electric field and result in the field emission enhancement effect. For a

homogeneous one-dimensional nanostructure, such as CNT, a long shape helps improve its field emission enhancement factor β. On the other hand, such shape means a relative larger resistance and a weaker capability of heat conduction. In ones' previous study based on CNTs, it has been derived that shorter emitter could lose more heat by heat conduction to substrate, thus carry higher emission current before vacuum breakdown.[45,46] This pair of contradiction impels people to find a balance in preparation. As for the metallic Mo nanoscrews in our case, the long length and sharp tip could enhance the field emission, while the large root diameter may decrease the resistance and promote the electrical transport and heat conduction. Moreover, the structure with protruding screwy thread may process an outstanding radiating capability due to its enlarged surface area.

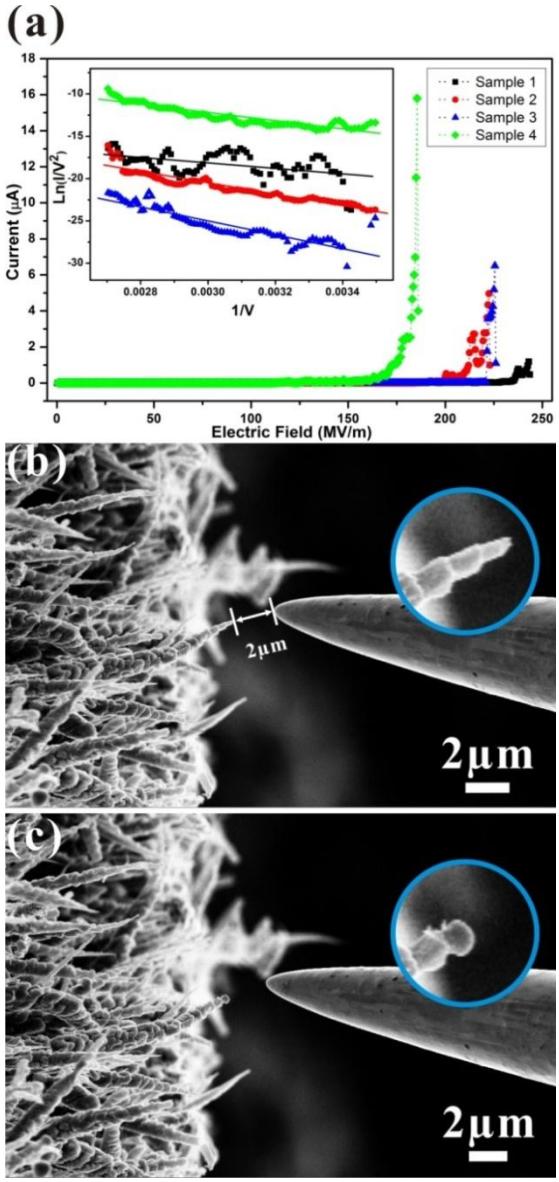

Figure 6. a) Field emission current versus electric field (*I–E*) characteristic curves of individual Mo nanoscrews and their corresponding FN plots at high electrical field region (inset). b,c) SEM images of a sample before and after vacuum breakdown, respectively.

SEM images in Figure 6b and 6c reveal the morphology of a Mo nanoscrew before and after vacuum breakdown. When the vacuum breakdown happened and the emission current reduced instantly, the whole nanoscrew remained undamaged and only the tip was fused (emphasized by the marking circle symbol), which could be related to the heat gathering around the tip at high electric field. These results indicate that the screw-like Mo nanostructure has a strong heat-carrying capability, which contributes to its large current field emission performance.

As expected from the Mo nanoscrews film, excellent field emission properties have been observed. Figure 7a shows the current versus electric field (*I–E*) curves of Mo nanoscrews film under a DC voltage driver mode, which was carried out with the cathode area of 0.02 cm^2 and the vacuum gap of 200 μm. The insets are the corresponding FN plots and the emission site distribution image (*I*~300 μA). The values of turn on field (E_{to}) and threshold field (E_{thr}), which are defined as the applied electric field to induce field emission current density of 10 μA cm^{-2} and 10 mA cm^{-2} respectively, are as low as 1.65 MV m^{-1} and 3.5 MV m^{-1}. These data are lower than other one-dimensional nanostructures, i.e., Cu_2S nanowires,[33] ZnO nanowires,[47] Mo nanowires,[7,25] Mo nanowalls,[27] MoO_2 nanowires,[7] MoO_3 nanowires,[7,48] MoO_2 nanorods,[49] pinaster-like MoO_2 nanoarrays,[50] MoO_3 nanobelts,[24] MoO_3 microbelts,[51] MoO_3 nanoflowers,[52] Mo oxide nanostars,[26] WO_3 nanowires[38] and $W_{18}O_{49}$ nanowires.[18] The value of a stable largest current density over 106.39 mA cm^{-2} were recorded and so far is higher than most of the emitter materials reported except for carbon nanotubes and MoO_3 nanobelts.[24,47] It shows that the Mo nanoscrews film has a high current capability for the potential applications in high current vacuum electron devices. In addition, the corresponding F-N plots exhibit approximately linear dependence, which mean that the field emission of the nanoscrews is consistent with the FN theory. When the current reached as high as 300 μA, the distribution uniformity of electron emission distribution sites was well. Moreover, the field emission stability curves of the nanoscrews under different emission current densities of 30 mA cm^{-2} and 50 mA cm^{-2} were measured (Figure 7b). One may see that the nanoscrews have a stable field emission with a fluctuation of only 0.46% in an hour of testing time, when the current density is as high as 50 mA cm^{-2}.

The field emission performance of the Mo nanoscrews film under a pulsed voltage driver has also been studied. Figure 7c shows the maximum input and output waveforms respectively recorded by oscilloscope, at the pulse width of 5 μs, the frequency of 2 kHz and the vacuum gap of 200 μm. The input waveform stands for the peak voltage of supplied pulse power, while the output one represents the obtained current of the external sampled resistance (20 Ω). The maximum emission current was recorded as 13.2 mA at a peak input voltage of 8 kV, and the corresponding maximum current density is about 0.66 A cm^{-2}. The pulse width has been found to have much effect on the field emission properties. Figure 7d reflects that the smaller the pulse width, the larger emission current of the nanoscrews can be got under constant vacuum gap and frequency.

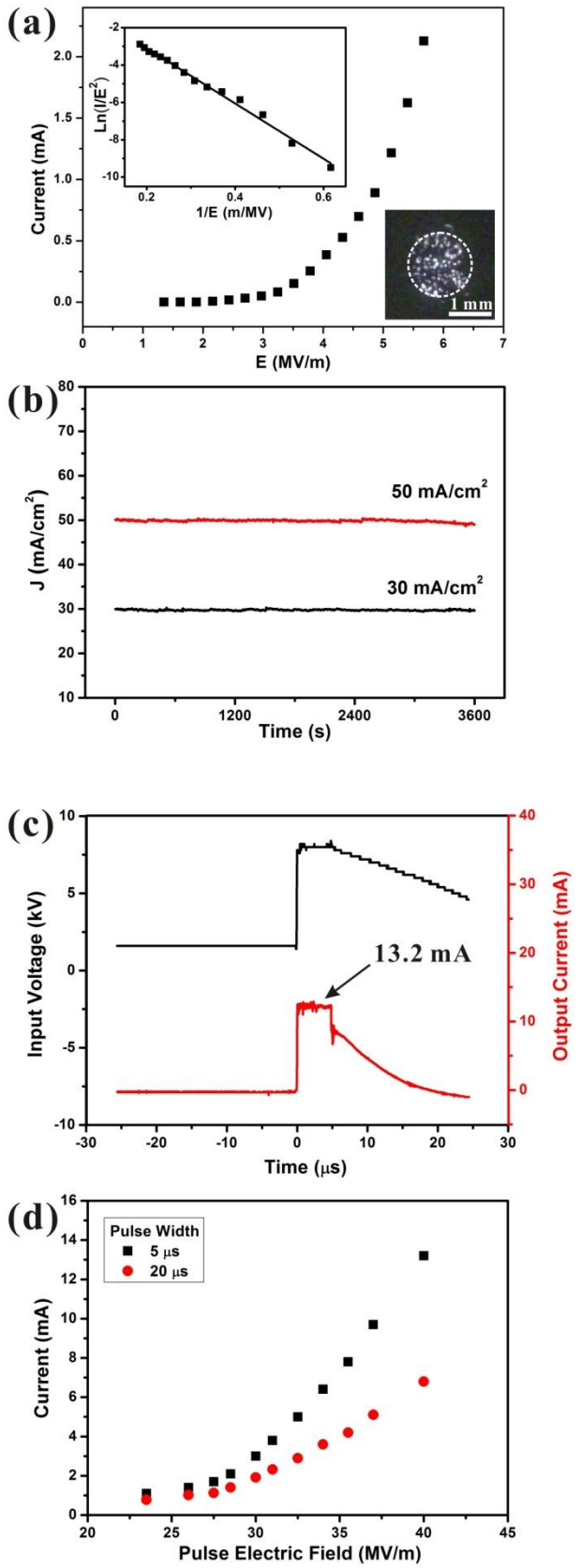

Figure 7. a) Field emission current versus electric field (*I–E*) curves of Mo nanoscrews film under DC voltage driver mode. The insets are its corresponding FN plots and the emission site distribution image (*I*~300 μA). b) The emission stability curves of the sample. c) The maximum input voltage waveform and the corresponding output current waveform of Mo nanoscrews film under pulsed voltage driver mode. The former marks the peak voltage of supplied pulse power, while the latter records the obtained maximum emission current. d) The *I–E* curves of the sample with different pulse width at the vacuum gap of 200 μm and the frequency of 2 kHz, respectively.

Conclusions

In summary, screw-like Mo nanostructures have been synthesized on stainless steel substrates based on a process of thermal vapor deposition. Each thread circle of a nanoscrew is formed by several crystalline Mo grains, which have a certain deflection with each other. The growth direction can be presented as the vector sum of all the nucleation directions of those Mo grains. The formation mechanism can be described as a spiral growth mode with the presence of various defects, which depends heavily on the degree of supersaturation (σ) of deposited Mo vapors. The electrical property measurements and field emission properties on single Mo nanoscrew show that its electrical conductivity should reach 3.44×10^{4} –7.74×10^{4} Ω^{-1} cm^{-1} and its maximum current can get 15.8 μA. Moreover, the Mo nanoscrews film is proved to have very large field emission current densities in both DC and pulsed voltage driver mode. Low turn-on field, good sites distribution and remarkable emission stability also have been recorded. These experimental results show that the high conductive molybdenum nanoscrews should be a potential application as cold cathode material for the high current vacuum electron devices.

Conflicts of interest statement

We confirm that there is no conflict of interest for our manuscript.

Acknowledgements

This work was supported by the National Key Basic Research Program of China (Grant No. 2013CB933601, 2010CB327703), the National Natural Science Foundation of China (Grant No.U1134006), the Science and Technology Department of Guangdong Province, and the Fundamental Research Funds for the Central Universities.

Notes and references

[a] *State Key Laboratory of Optoelectronic Materials and Technologies, Guangdong Province Key Laboratory of Display Material and Technology, and School of Physics and Engineering, Sun Yat-Sen University, Guangzhou 510275, P. R. China. Fax: 86(20)84037855; Tel: 86(20)84110916; E-mail: stsdsz@mail.sysu.edu.cn*

1 S. Iijima, *Nature*, 1991, **354**, 56.
2 J. Westwater, D. P. Gosain, S. Tomiya, S. Usui and H. Ruda, *J. Vac. Sci. Technol. B*, 1997, **15**, 554.
3 Y. Y. Wu and P. D. Yang, *Chem. Mater*, 2000, **12**, 605.
4 J. H. Zhan, X. G. Yang, D. W. Wang, S. D. Li, Y. Xie, Y. Xia and Y. Qian, *Adv. Mater*, 2000, **12**, 1348.
5 M. H. Huang, Y. Wu, H. Feick, N. Tran, E. Weber and P. D. Yang, *Adv. Mater*, 2001, **13**, 113.
6 Z. W. Pan, Z. R. Dai, C. Ma and Z. L. Wang, *J. Am. Chem. Soc*, 2002, **124**, 1817.

7 J. Zhou, N. S. Xu, S. Z. Deng, J. Chen, J. C. She and Z. L. Wang, *Adv. Mater*, 2003, **15**, 1835.
8 Y. Cui, X. Duan, J. Hu and C. M. Lieber, *J. Phys. Chem. B*, 2000, **104**, 5213.
9 X. Duan, Y. Huang, Y. Cui, J. Wang and C. M. Lieber, *Nature*, 2001, **409**, 66.
10 Y. Huang, X. Duan, Y. Cui, L. Lauhon, K. Kim and C. M. Lieber, *Science*, 2001, **294**, 1313.
11 M. H. Huang, S. Mao, H. Feick, H. Q. Yan, Y. Y. Wu, H. Kind, E. Weber, R. Russo and P. Yang, *Science*, 2001, **292**, 1897.
12 Z. L. Wang and J. H. Song, *Science*, 2006, **342**, 242.
13 Z. W. Pan, Z. R. Dai and Z. L. Wang, *Science*, 2001, **291**, 1947.
14 Y. Zhang, K. Suenaga, C. Colliex and S. Iijima, *Science*, 1998, **281**, 973.
15 K. S. Novoselov, A. K. Geim, S. V. Morozov, D. Jiang, Y. Zhang, S. V. Dubonos, I. V. Grigorieva and A. A. Firsov, *Science*, 2004, **306**, 666.
16 H. S. S. Ramakrishna Matte, A. Gomathi, A. K. Manna, D. J. Late, R. J. Datta, S. K. Pati and C. N. R. Rao, *Angew. Chem. Int. Ed*, 2010, **122**, 4153.
17 Y. H. Wu, P. W. Qiao, T. C. Chong and Z. X. Shen, *Adv. Mater*, 2002, **14**, 64.
18 J. Zhou, L. Gong, S. Z. Deng, J. Chen, J. C. She, N. S. Xu, R. S. Yang and Z. L. Wang, *Appl. Phys. Lett*, 2005, **87**, 223108.
19 F. Hao, C. L. Nehl, J. H. Hafner and P. Nordlander, *Nano Lett*, 2007, **7**, 729.
20 X. Y. Kong and Z. L. Wang, *Nano Lett*, 2003, **3**, 1625.
21 A. G. Worthing, *Phys. Rev*, 1925, **25**, 846.
22 A. G. Worthing, *Phys. Rev*, 1926, **28**, 190.
23 C. A. Spindt, I. Brodie, L. Humphrey and E. R. Westerberg, *J. Appl. Phys*, 1976, **47**, 5248.
24 Y. B. Li, Y. S. Bando, D. Golberg and K. Kurashima, *Appl. Phys. Lett*, 2002, **81**, 5048.
25 J. Zhou, S. Z. Deng, L. Gong, Y. Ding, J. Chen, J. X. Huang, J. Chen, N. S. Xu and Z. L. Wang, *J. Phys. Chem. B*, 2006, **110**, 10296.
26 A. Khademi, R. Azimirad, A. A. Zavarian and A. Z. Moshfegh, *J. Phys. Chem. C*, 2009, **113**, 19298.
27 Y. Shen, S. Z. Deng, Y. Zhang, F. Liu, J. Chen and N. S. Xu, *Nanoscale. Res. Lett*, 2012, **7**, 463.
28 W. K. Burton, N. Cabrera and F. C. Frank, *Phil. Trans. R. Soc. Lond. A*, 1951, **243**, 299.
29 T. Akasaka, Y. Kobayashi and M. Kasu, *Appl. Phys. Lett*, 2010, **97**, 141902.
30 F. C. Frank, *Adv. Phys*, 1952, **1**, 91.
31 W. B. Hillig, *Acta Metall*, 1966, **14**, 1868.
32 T. W. Ebbesen, H. J. Lezec, H. Hiura, J. W. Bennett, H. F. Ghaemi and T. Thio, *Nature*, 1996, **382**, 54.
33 J. Chen, S. Z. Deng, N. S. Xu, S. H. Wang, X. G. Wen, S. H. Yang, C. L. Yang, J. N. Wang and W. K. Ge, *Appl. Phys. Lett*, 2002, **80**, 3620.
34 P. R. Shao, S. Z. Deng, J. Chen, J. Chen and N. S. Xu, *J. Appl. Phys*, 2011, **109**, 023710.
35 Y. Z. Long, Z. J. Chen, W. L. Wang, F. L. Bai, A. Z. Jin and C. Z. Gu, *Appl. Phys. Lett*, 2005, **86**, 153102.
36 J. C. She, Z. M. Xiao, Y. H. Yang, S. Z. Deng, J. Chen, G. W. Yang and N. S. Xu, *ACS Nano*, 2008, **2**, 2015.
37 S. L. Shi, X. Y. Xue, P. Feng, Y. G. Liu, H. Zhao and T. H. Wang, *J. Cryst. Growth*, 2008, **310**, 462.
38 F. Liu, L. Li, F. Y. Mo, J. Chen, S. Z. Deng and N. S. Xu, *Cryst. Growth. Des*, 2010, **10**, 5193.
39 F. Liu, Z. J. Su, L. Li, F. Y. Mo, S. Y. Jin, S. Z. Deng, J. Chen, C. M. Shen, H. J. Gao and N. S. Xu, *Adv. Funct. Mater*, 2010, **20**, 1994.
40 F. Liu, C. M. Shen, Z. J. Su, X. L. Ding, S. Z. Deng, J. Chen, N. S. Xu and H. J. Gao, *J. Mater. Chem*, 2010, **20**, 2197.
41 Y. Tian, H. L. Lu, J. F. Tian, C. Li, C. Hui, X. Z. Shi, Y. Huang, C. M. Shen and H. J. Gao, *Appl. Phys. Lett*, 2012, **100**, 103112.
42 Y. Huang, F. Liu, Q. Luo, Y. Tian, Q. Zou, C. Li, C. M. Shen, S. Z. Deng, C. Z. Gu, N. S. Xu and H. J. Gao, *Nano Res*, 2012, **5**, 896.
43 H. C. Wu, T. C. Hou, Y. L. Chueh, L. J. Chen, H. T. Chiu and C. Y. Lee, *Nanotechnology*, 2010, **21**, 455601.
44 Y. Wei, C. G. Xie, K. A. Dean and B. F. Coll, *Appl. Phys. Lett*, 2001, **79**, 4527.
45 N. Y. Huang, J. C. She, J. Chen, S. Z. Deng, N. S. Xu, H. Bishop, S. E. Huq, L. Wang, D. Y. Zhong, E. G. Wang and D. M. Chen, *Phys. Rev. Lett*, 2004, **93**, 075501.
46 M. Sveningsson, K. Hansen, K. Svensson, E. Olsson and E. E. B. Campbell, *Phys. Rev. B*, 2005, **72**, 085429.
47 C. J. Lee, T. J. Lee, S. C. Lyu, Y. Zhang, H. Ruh and H. J. Lee, *Appl. Phys. Lett*, 2002, **81**, 3648.
48 J. Zhou, S. Z. Deng, N. S. Xu, J. Chen and J. C. She, *Appl. Phys. Lett*, 2003, **83**, 2653.
49 J. G. Liu, Z. J. Zhang, C. Y. Pan, Y. Zhao, X. Su, Y. Zhou and D. P. Yu, *Mater. Lett*, 2004, **58**, 3812.
50 J. Y. Zhang, Y. G. Liu, S. L. Shi, Y. G. Wang and T. H. Wang, *Chin. Phys. B*, 2008, **17**, 4333.
51 D. M. Ban, S. Z. Deng, N. S. Xu, J. Chen, J. C. She and F. Liu, *J. Nanomater*, 2010, **1155**, 136860.
52 G. D. Wei, W. P. Qin, D. S. Zhang, G. F. Wang, R. J. Kim, K. Z. Zheng and L. L. Wang, *J. Alloy. Compd*, 2009, **481**, 417.